THE LANCET
Planetary Health

Supplementary appendix

This appendix formed part of the original submission and has been peer reviewed. We post it as supplied by the authors.

Supplement to: Lowe R, Lee SA, O'Reilly KM, et al. Combined effects of hydrometeorological hazards and urbanisation on dengue risk in Brazil: a spatiotemporal modelling study. *Lancet Planet Health* 2021; **5:** e209–19.

Combined effects of hydrometeorological hazards and urbanisation on dengue risk in Brazil: a spatiotemporal modelling study

Appendix

Study area and data

Brazil is now the sixth most populated country in the world with more than 209 million inhabitants. It has the largest economy in South America but since 2015 it has also been the most unequal country in the region in terms of wealth.[1] Due to variations in altitude, dominance of air masses, atmospheric circulation, proximity to the Atlantic Ocean and vegetation type, Brazil can be divided into distinct climatic and ecological zones spanning 8.5 million km^2. The Amazon rainforest is dominated by a hot and humid climate and rivers with permanent flow; the Caatinga biome features a hot semi-arid climate while the Atlantic forest experiences a mixture of tropical and subtropical climates with marked dry seasons (Fig A1a and Fig A1b). Brazil is comprised of five geo-political regions (North, Northeast, Southeast, South, Central-West, Fig A1c), which further divide into 26 states and a Federal District, where the capital city Brasília is located. There are 5 570 municipalities organized in 558 microregions, which consist of groups of municipalities surrounding a larger city. The median microregion area is 5 548 km^2 with an interquartile range of 2 862-15 959 km^2.

Disease surveillance and demographic data

We obtained monthly notified dengue cases between January 2001 and December 2019 for each of the 558 microregions of Brazil from the Notifiable Diseases Information System (SINAN), freely available via the Ministry of Health Information Department (DATASUS).[2] Cases were aggregated by month of first symptom and microregion of residence. Dengue cases are considered confirmed if they test positive in a laboratory or, more commonly, based on the Ministry of Health's syndromic definition. That is, patients living or travelling in an area where dengue transmission is occurring or the vector *Ae. aegypti* is present within the last 14 days, experiencing fever, for between 2 and 7 days, and at least 2 other symptoms of dengue. It is not possible to confirm all cases in a laboratory, particularly during epidemics. Just 25% of suspected dengue cases were laboratory tested in the first 20 weeks of 2020, and only half of those were confirmed.[3]

Methods

Model description

Spatiotemporal Bayesian hierarchical model

We specified a spatiotemporal Bayesian hierarchical mixed model where the response consists of monthly counts of confirmed dengue cases for all 558 Brazilian microregions over a 19-year period, from January 2001 to December 2019. Counts of dengue cases, y_{st} (s = 1, …, 558, t = 1, …, 228), were assumed to follow a negative binomial distribution

$$y_{st} \mid \mu_{st}, \kappa \sim \text{NegBin}(\mu_{st}, \kappa)$$

$$\log(\mu_{st}) = \log(p_{sa(t)}) + \log(\rho_{st})$$

where μ_{st} is the corresponding distribution mean, which is equal to the yearly population per 100 000 $p_{s\,a(t)}$, where a(t) = 2001, …, 2019, multiplied by the unknown dengue incidence rate estimate ρ_{st} for microregion s at time t, and κ is the scale (or overdispersion) parameter.[4] Note, we also tested a Poisson distribution baseline model, but goodness of fit criteria indicated a negative binomial formulation was necessary to account for residual overdispersion in addition to spatiotemporal random effects (see below for details). Population effects were accounted for by including log population per 100 000 in the model as an offset at the linear predictor scale (which is assigned a coefficient of one). The model equation can then be rearranged such that ρ_{st} is equivalent to the dengue incidence rate per 100 000 population.

We first constructed a baseline model comprising spatiotemporal random effects to account for seasonality at the state level and interannual variability in spatial dependency structures. Seasonality and seasonal autocorrelation were accounted for by including a state-level random effect per calendar month in the model. A cyclic first order random walk prior was used, which allows each month to depend on the previous month, with no discontinuity between January in year a(t) and December in year a(t)-1. Through a sensitivity analysis, geo-political region or biome were found to be too coarse to capture adequate variation in the annual cycle, while including a monthly random effect at the microregion level would have resulted in overfitting. Interannual variability and long-term trends were accounted for via yearly spatial random effects, which allow for any annual trends to differ throughout the time period in a given location. Unstructured random effects allowed for independent area-specific noise, such as differences in vector ecology, healthcare access and reporting rates. Structured spatial random effects allow for dependency between neighbouring regions due to shared environmental and socio-economic characteristics, such as climatic zone, land use, health care access and human movement.

Model parameters were estimated in a Bayesian framework, using Integrated Nested Laplace Approximation (INLA, www.r-inla.org)[5,6] in R version 4.0.2. INLA is straightforward to use for full Bayesian inference in disease mapping and avoids computationally intensive Markov chain Monte Carlo techniques.[7] Parameter uncertainty was accounted for by assigning prior distributions to the parameters. State-specific seasonality was included using autocorrelated random effects for calendar month, m(t) = 1, …, 12 (January to December), for each state (27 in total). This state-specific monthly random effect, $\beta_{s(s)\,m(t),}$ was assigned a cyclic random walk of order one, or first difference prior distribution, in which each effect is derived from the immediately preceding effect,

$$\beta_{s(s)\,m(t)} - \beta_{s(s)\,m(t)-1} \sim N(0, \sigma^2_{\beta}),$$

where $\beta_{s(s)1}$ represents the parameter estimate for the month of January for state s(s). Note, the cyclic nature of the prior allows the last effect to neighbour both the previous and first effect, allowing dengue incidence in January to depend on dengue incidence in December from the previous year. Figure A6 shows the marginal posterior distribution for the monthly random effects in each state using the best fitting model (drought severity - urban model, see article). To account for interannual variability due to unknown and unmeasured features in space (e.g. introduction of a new dengue serotype or similar arbovirus in a particular time and place, change in reporting practices, etc.) and long-term trends, we interacted year, a(t) = 2001, …, 2019, with microregion-specific spatially

unstructured and structured random effects. For the spatial component we use a modified Besag-York-Mollie (BYM) model with a scaled spatial component, which facilitates assignment of interpretable hyperpriors and makes these transferable between different geographical settings.[8] The classical BYM model comprises an unstructured spatial random effect to account for independent area-specific noise and a conditional autoregressive model (often referred to as the CAR prior), where the spatial effect of a particular region depends on the effects of all neighbouring regions.[9] The modified BYM model consists of one precision parameter and one mixing parameter. The precision parameter represents the marginal precision and controls the variability explained by the spatial effect.[8] The mixing parameter distributes existing variability between an unstructured and structured component, $\varphi_{s\ a(t)} + \upsilon_{s\ a(t)}$. The unstructured component helps account for unknown or unobserved confounding factors, such as population immunity, quality of healthcare services and local vector control interventions. It introduces an extra source of variability (a latent effect) into the model, which can assist in modelling overdispersion, in addition to the single-scale parameter in the negative binomial model. The structured component assumes that spatial dependency exists if regions share a border, acting as a surrogate for spatial autocorrelation that arises between nearby regions due to shared environmental or socio-economic characteristics. For all random effects, we used the Penalized Complexity (PC) prior [10] for the precision $\tau = 1/\sigma^2$, so that $Pr(1/\sqrt{\tau} > 0.5) = 0.01$.[10] The main benefit of the modified BYM model is that it allows for an intuitive parameter interpretation and facilitates prior assignment (see Riebler et al.[8] for further details).

Distributed lag nonlinear models

Distributed lag nonlinear models were used to explore possible non-linear and delayed associations between dengue incidence rates and climate indicators. The distributed lag nonlinear model (DLNM) framework is based on the definition of a cross-basis, a bi-dimensional space of functions specifying the dependency along the space of the predictor and along lags.[11] The cross-basis functions are built by combining a standard exposure–response function f(x), to express the potentially nonlinear relationship along the dimension of the climate predictors, with a lag-response function w(*l*), for the temporal dimension. Their combination in a bi-dimensional exposure–lag–response function f.w(x, *l*) allows the model to flexibly estimate both the intensity and timing of past exposures. The delayed effects of the climate indicators were assessed up to six months with natural cubic splines selected for both the exposure (with two equally spaced knots) and the lag dimensions (with one internal knot at the 50th percentile for temperature and two equally spaced knots for the drought severity index), to allow enough flexibility to capture potentially complex associations between climatic indicators and their delayed impact on dengue risk. The temperature exposure index was chosen as monthly average daily minimum temperature (T_{min}). We assessed this choice in sensitivity analysis, replacing minimum with maximum temperature (see Table A1). The self-calibrating Palmer drought severity index (PDSI) was chosen as an intuitive and widely used measure of dryness.[12] The T_{min} DLNM and PDSI DLNM were obtained by the combination of the exposure–response and lag–response functions, with associated parameters representing the whole exposure-lag-response surface, expressed as relative risk.[11] The number of coefficients in the cross-basis matrix represents the degrees of freedom (df) used to model the association. The T_{min} DLNM was defined by nine cross-basis variables (3 df [natural cubic spline with 1 knot + 1] in the exposure-response dimension multiplied by 3 df [natural cubic spline with 1 knot + intercept + 1] in the lag-response dimension) and the PDSI DLNM by twelve cross-basis variables (3 df [natural cubic spline with

2 knots + 1] in the exposure-response dimension multiplied by 4 df [natural cubic spline with 2 knots + intercept + 1] in the lag-response dimension).

To assess the impact of drought on underlying socio-economic conditions, we extended the drought severity model to a space-varying DLNM by including a linear interaction between the percentage of residents living in urban areas (i.e. level of urbanisation) and the PDSI cross-basis variables.[13] We obtained the percentage of residents living in urban areas for each microregion from the IBGE 2010 census.[14] To simplify the interpretation and make use of the standard DLNM software, we directly defined main and interaction terms before including them in the Bayesian hierarchical model. The main effects are represented by the cross-basis variables described above; interaction terms were produced by multiplying the main terms with the urbanisation variable. We centred the urbanisation variable at three different levels ranging from highly urbanised to more rural: high (upper quartile = 87%), intermediate (median = 73%) and low (lower quartile = 58%) levels of urbanisation. This resulted in an additional 13 variables: twelve cross-basis variables and the continuous urbanisation variable as a fixed effect, in each parameterisation of the drought severity – urban model. We also tested a linear interaction between the frequency of reported water supply shortages, centred at high (upper quartile = 0.53), intermediate (median = 0.33) and low (lower quartile = 0.16) frequency levels, and PDSI cross-basis variables. In the interaction models, the bi-dimensional exposure-lag-response changes depending on the value of the interactive variable. The idea of subtracting a value of interest (e.g., upper quartile of the distribution) is to define a parameterisation in which the interaction term (cross-basis multiplied by the interactive variable) is 0 for that value. Therefore, the predictions obtained by using the main term (standard cross-basis object) can be interpreted as the exposure-lag-response for the upper quartile (or any predefined) value. By changing the centring point, the model stays the same, but is defined by a different parameterisation.

We calculated goodness of fit measures to select the best fitting model, including the deviance information criterion (DIC)[15] which balances model accuracy against complexity, by penalising for the number of effective parameters in model. For each observation, we calculated the conditional predictive ordinates (CPO)[16], which is a cross-validatory criterion for model assessment. For each observation, the CPO is the posterior probability of observing that observation when the model is fit using all data expect that observation. We summarised the CPO by calculating the cross validated (CV) log score.[17] For both the DIC and the CV log score, smaller values indicate better fitting models. We also calculated the difference in mean absolute error (MAE) between the baseline model and each new candidate model, to identify the proportion of microregion for which more complex models improved model fit.[18]

The best estimate of the dengue incidence rate was as follows:

$$y_{st} \mid \mu_{st}, \kappa \sim \text{NegBin}(\mu_{st}, \kappa)$$

$$\log(\mu_{st}) = \log(p_{s\,a(t)}) + \log(\rho_{st})$$

$$\log(\rho_{st}) = \alpha + \beta_{s(s)\,m(t)} + \varphi_{s\,a(t)} + \upsilon_{s\,a(t)} + \text{f.w}(x_{1st}, l) + \text{f.w}(x_{2st}, l) + \text{f.w}(x_{2st}, l) \cdot v_u$$

where $\log(\rho_{st})$ comprised an intercept, α, state-specific monthly random effects, $\beta_{s(s)\ m(t)}$, year-specific spatially unstructured, $\varphi_{s\ a(t)}$, and structured, $\upsilon_{s\ a(t)}$, random effects at the microregion level and nonlinear exposure-lag functions $f.w(x_{ist}, l)$ of minimum temperature, x_{1st}, and the Palmer drought severity index, x_{2st}, with lags, l, from zero to six months. An additional space varying DLNM, $f.w(x_{2st}, l) \cdot v_u$, was added to account for differences in relative risk due to drought severity given different level of urbanisation, where v_u is a continuous variable of the % population residing in urban areas. We also tested a space-varying DLNM, $f.w(x_{2st}, l) \cdot v_w$, to account for differences according to the frequency of water supply shortages, where v_w is the frequency of reported water supply shortages per microregion over a 17-year period (2000 – 2016).

To analyse output from the best fitting model, posterior predictive distributions of the response variable were simulated using samples from the posterior distribution of the parameters and hyperparameters from the model, fitted 19 x 12 times, leaving out a month per year each time.[19] The posterior predictive distribution of dengue cases $\mathbf{y_{st}}$ was estimated by drawing 1000 random values from a negative binomial distribution with mean corresponding to the elements of $\boldsymbol{\mu_{st}}$ and scale parameter corresponding to the elements of the overdispersion parameter $\boldsymbol{\kappa}$ estimated from the model for the prediction month of interest. This step allows for uncertainty in the response variable, given the model parameters. We therefore generated posterior predictive distributions for each timestep across all microregions and compared posterior predictive summaries (e.g. median and 95% credible interval) to observed cases ().

Data and code

All data used in this study is open access and freely available via the internet. The data and code used to produce the analysis can be found here: https://github.com/drrachellowe/hydromet_dengue.

Table A1. Model adequacy results for models of increasing complexity

The deviance information criterion (DIC) and the cross-validated (CV) mean logarithmic score for models of increasing complexity. Lower scores indicate a better fitting model.

Model	Dengue incidence rate estimate $\log(\rho_{st})$	DIC	CV mean log score
Baseline	$\alpha + \beta_{s(s)\,m(t)} + \varphi_{s\,a(t)} + \upsilon_{s\,a(t)}$ Spatiotemporal random effects	830559	3.315
T_{min}	$\alpha + \beta_{s(s)\,m(t)} + \varphi_{s\,a(t)} + \upsilon_{s\,a(t)} + f.w(x_{1st}, l)$ Base model + T_{min} DLNM	828515	3.303
T_{max}	$\alpha + \beta_{s(s)\,m(t)} + \varphi_{s\,a(t)} + \upsilon_{s\,a(t)} + f.w(x_{1st}, l) + f.w(x_{2st}, l)$ Base model + T_{max} DLNM	829163	3.305
PDSI	$\alpha + \beta_{s(s)\,m(t)} + \varphi_{s\,a(t)} + \upsilon_{s\,a(t)} + f.w(x_{1st}, l)$ Base model + PDSI DLNM	829103	3.308
T_{min} + PDSI	$\alpha + \beta_{s(s)\,m(t)} + \varphi_{s\,a(t)} + \upsilon_{s\,a(t)} + f.w(x_{1st}, l) + f.w(x_{2st}, l)$ Base model + T_{min} DLNM + PDSI DLNM	827095	3.296
T_{max} + PDSI	$\alpha + \beta_{s(s)\,m(t)} + \varphi_{s\,a(t)} + \upsilon_{s\,a(t)} + f.w(x_{1st}, l) + f.w(x_{2st}, l)$ Base model + T_{max} DLNM + PDSI DLNM	827833	3.299
T_{min} + PDSI*urban	$\alpha + \beta_{s(s)\,m(t)} + \varphi_{s\,a(t)} + \upsilon_{s\,a(t)} + f.w(x_{1st}, l) + f.w(x_{2st}, l) \cdot v_u$ Base model + T_{min} DLNM + PDSI DLNM*urbanisation	826978	3.296
T_{min} + PDSI*water	$\alpha + \beta_{s(s)\,m(t)} + \varphi_{s\,a(t)} + \upsilon_{s\,a(t)} + f.w(x_{1st}, l) + f.w(x_{2st}, l) \cdot v_w$ Base model + T_{min} DLNM + PDSI DLNM*water shortage	826936	3.296

CV: cross-validated; DIC: deviance information criterion; DLNM: Distributed Lag Nonlinear Model; T_{min}: minimum temperature; T_{max}: maximum temperature; PDSI: Palmer drought severity index.

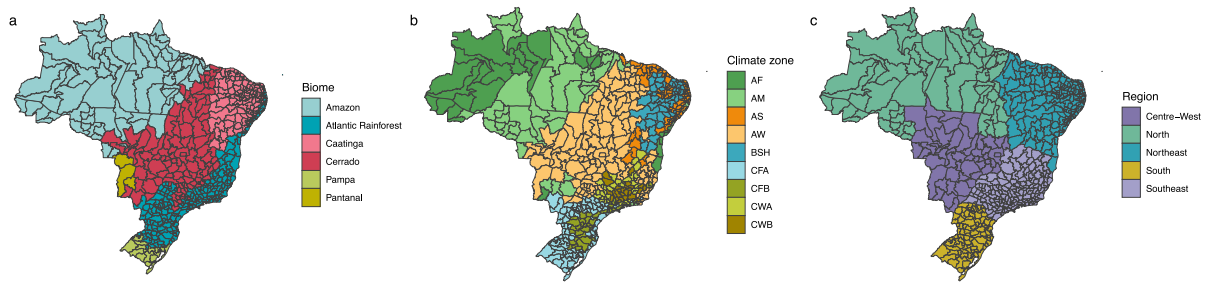

Figure A1: Brazilian geopolitical regions and biomes

Location of (a) six biomes (Amazon, Atlantic Rainforest, Caatinga, Cerrado, Pampa and Pantanal), (b) nine Köppen climate classification groups (Af: Tropical rainforest climate, Am: Tropical monsoon climate, As: Tropical savanna climate with dry-summer characteristics, Aw: Tropical savanna climate with dry-winter characteristics, Bsh: Hot semi-arid climate, Cfa: Humid sub-tropical climate, Cfb: oceanic climate, Cwa: Dry-winter humid subtropical climate, Cwb: Dry-winter subtropical highland climate) and (c) five geo-political regions (Centre-West, North, Northeast, Southeast, South).

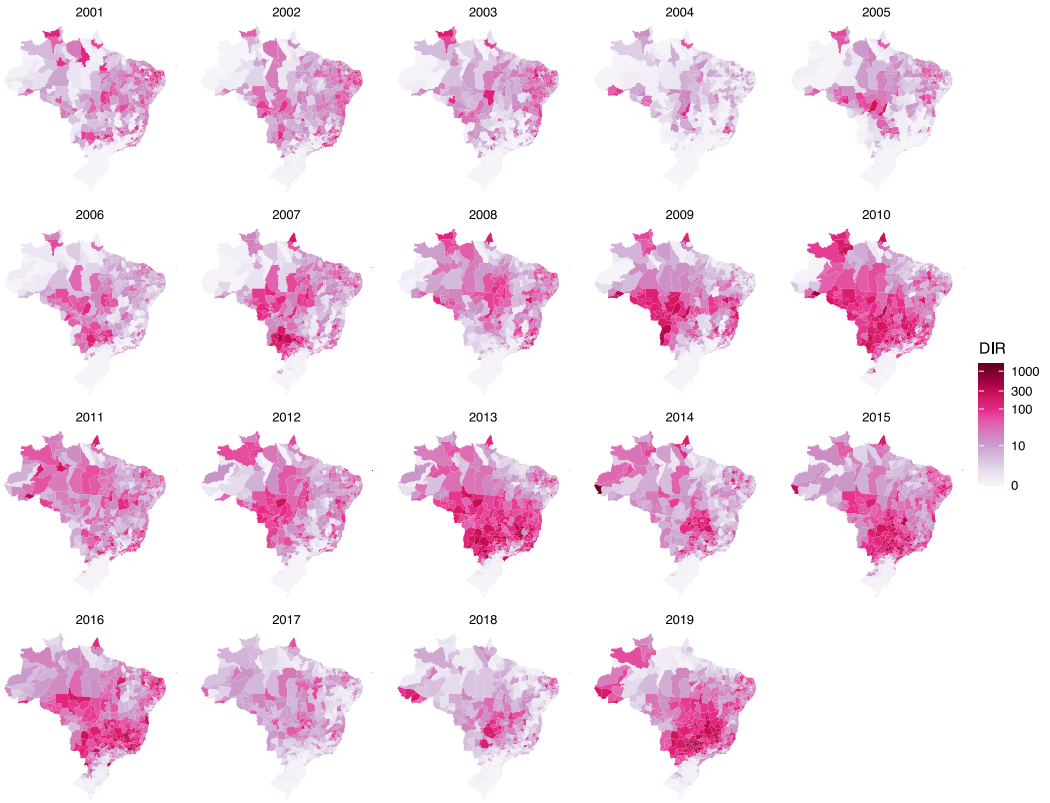

Figure A2: Yearly dengue incidence rate 2001 – 2019

Dengue incidence rate (DIR) per 100 000 people per year from 2001 to 2019 for the 558 microregions in Brazil.

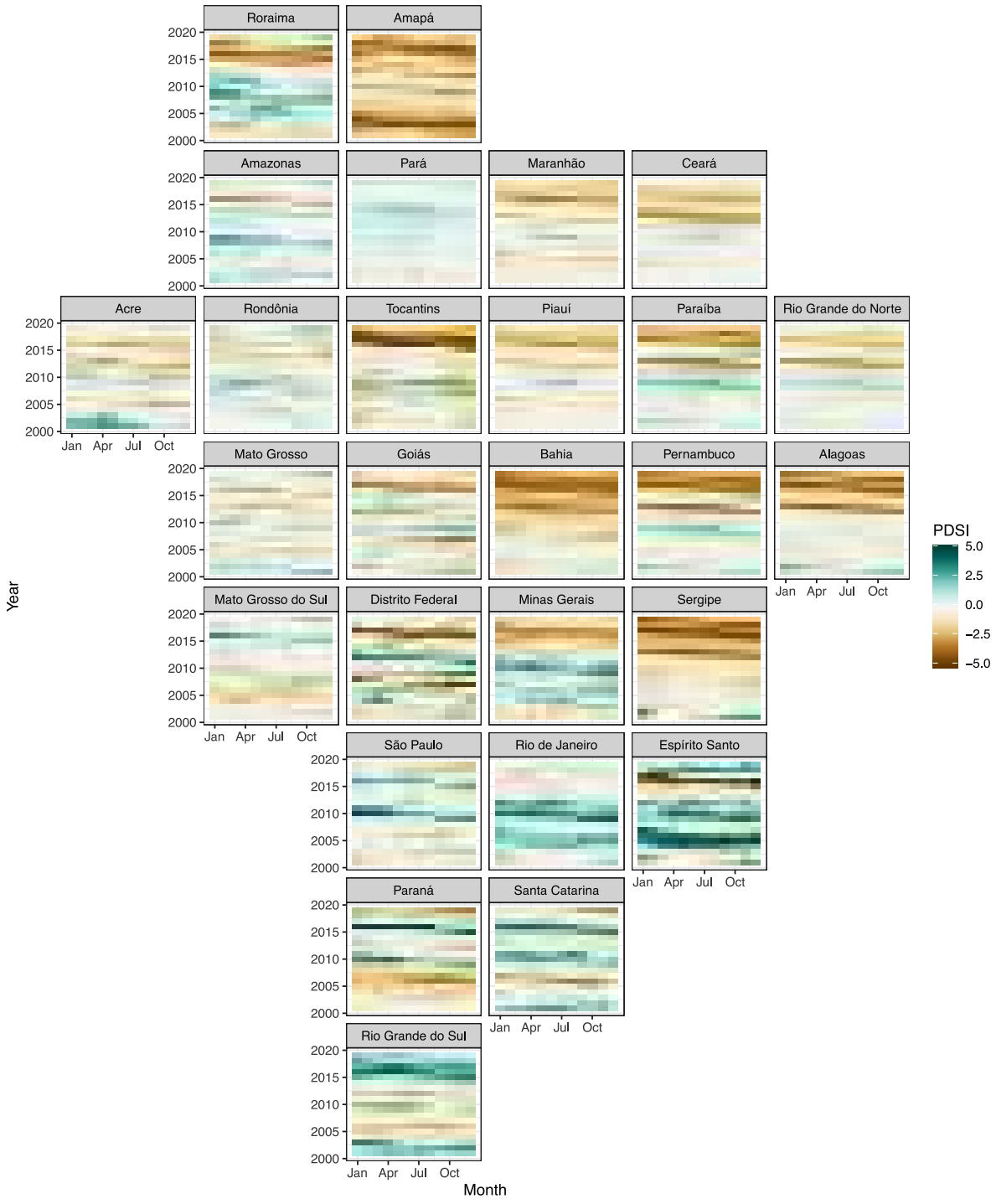

Figure A3: Spatial and temporal variation in the drought severity index in Brazil, by state

Monthly self-calibrated Palmer drought severity index (PDSI) between January 2001 and December 2019 aggregated at the state level. States are ordered by their geographical location. Data source: CRU TS Version 4.04.[20]

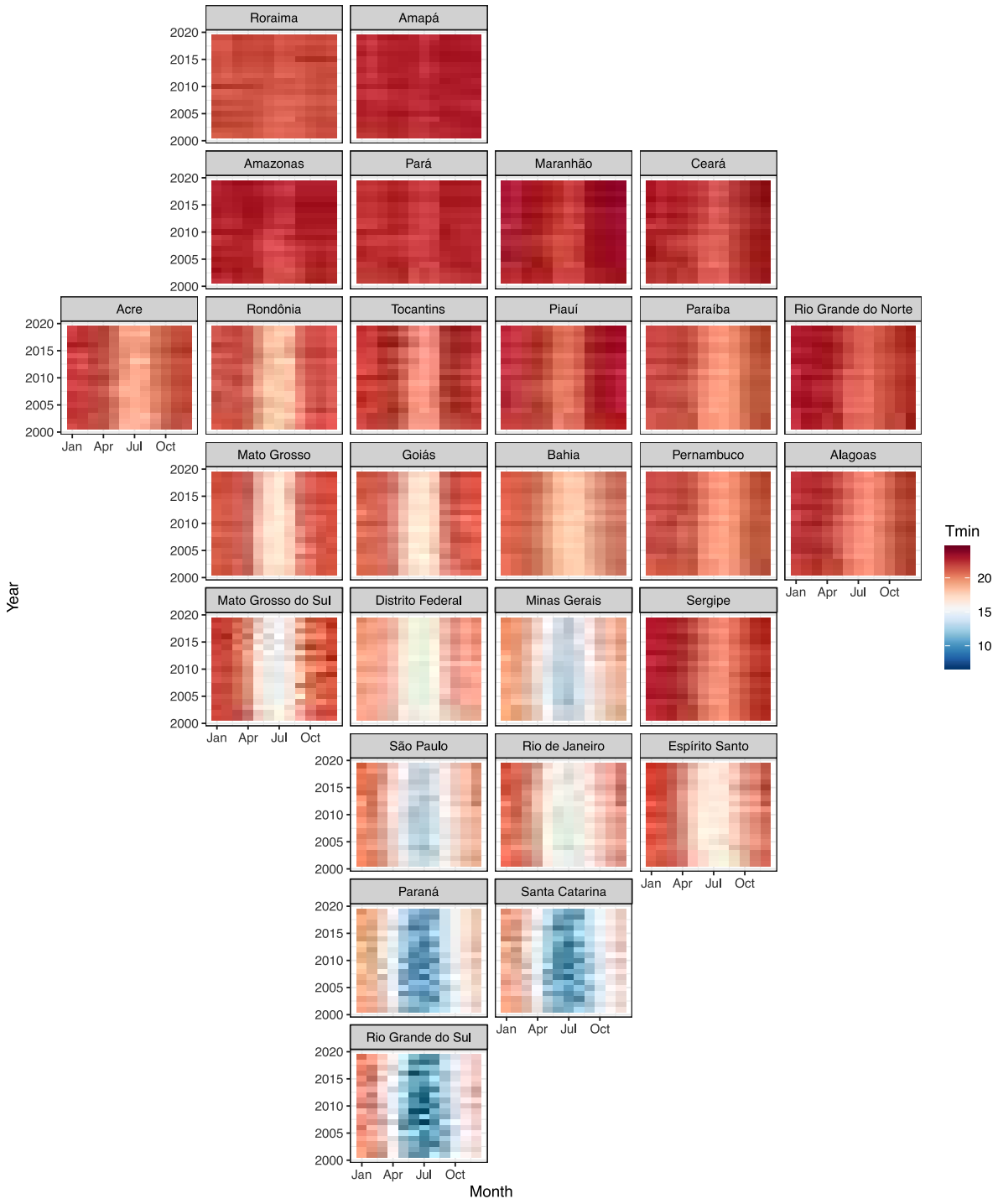

Figure A4: Spatial and temporal variation in minimum temperature in Brazil, by state

Monthly minimum temperature (T_{min}) between January 2001 and December 2019 aggregated at the state level. States are ordered by their geographical location. Data source: CRU TS Version 4.04.[20]

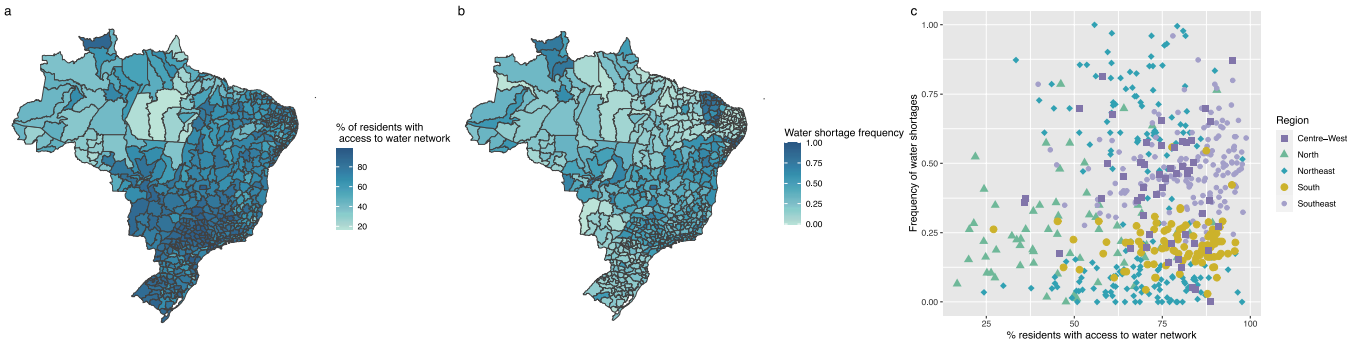

Figure A5: Water access and water shortages

(a) Percentage (%) of residents per microregion with access to the water network according to the 2010 census, (b) frequency of reported water shortages between 2000-2016, (c) frequency of water shortages per microregion against % of residents with access to the water network, stratified by geo-political region.

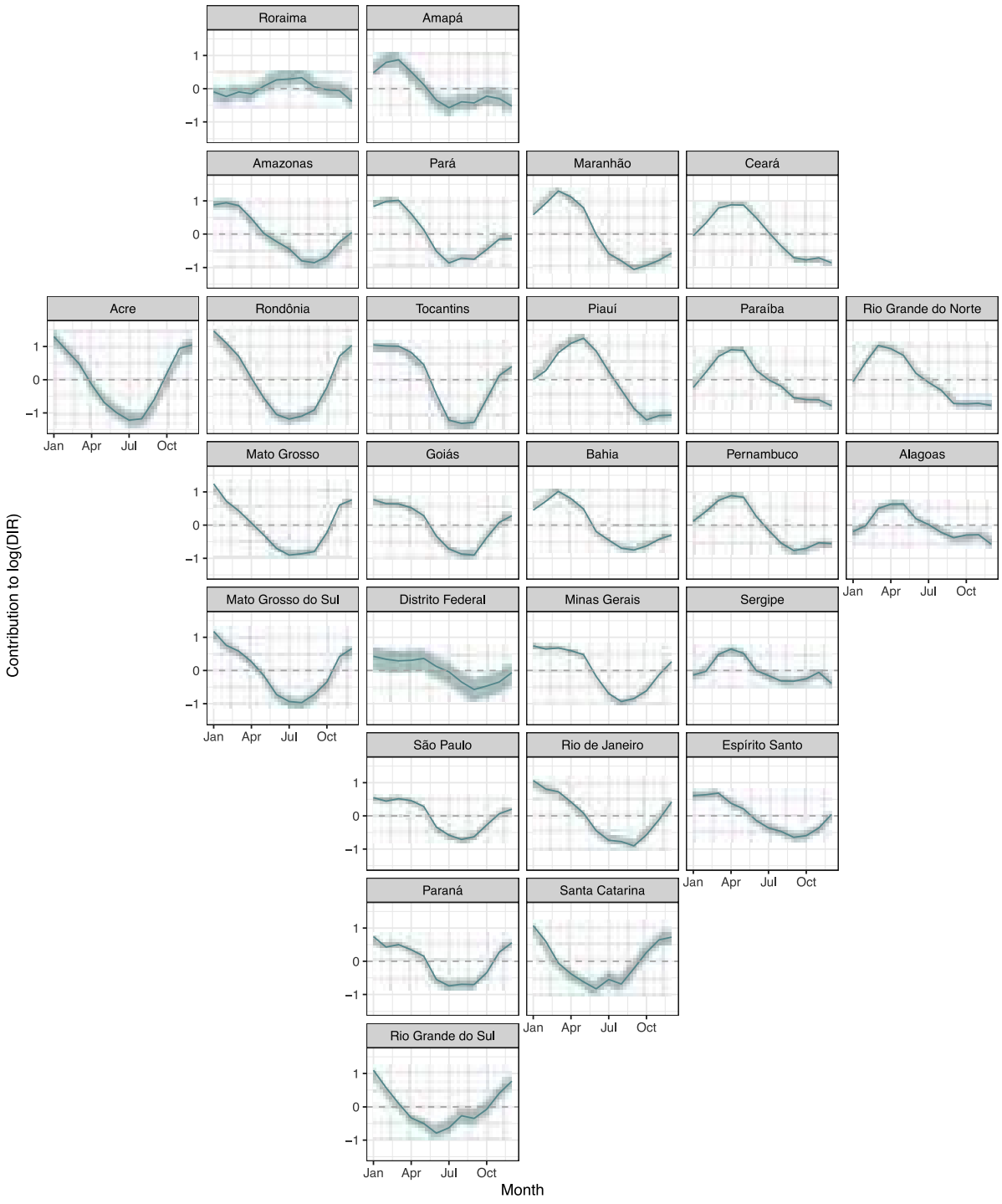

Figure A6: Posterior distributions of state-specific autocorrelated monthly random effects

Posterior mean (solid curve) and 95% credible interval (shaded area) of marginal posterior distribution of the autocorrelated month random effects (e.g., the annual cycle) at the linear predictor scale from January to December for the 26 states and 1 federal district (Distrito Federal) in Brazil. This shows the contribution of the random effects to the log of the dengue incidence rate using the drought severity - urban model. States are ordered by their geographical location.

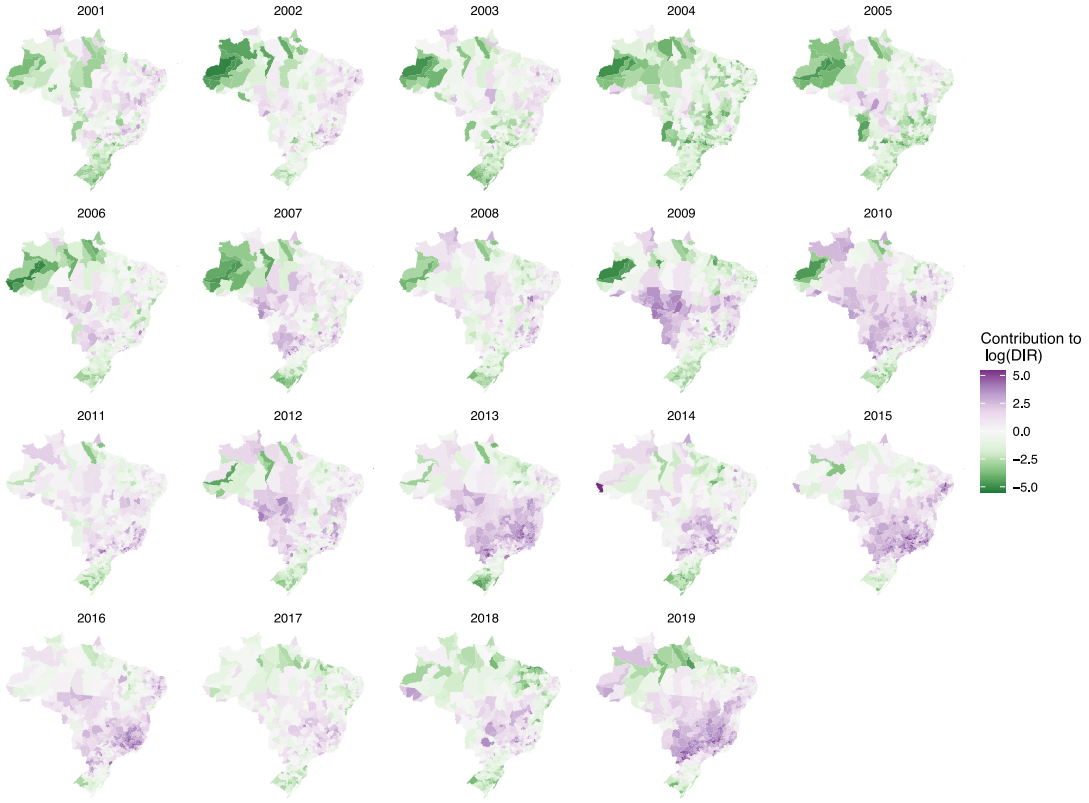

Figure A7: Contribution of year-specific spatial random effects to dengue incidence rate estimates

Marginal posterior mean of the combined spatially structured and unstructured random effects at the linear predictor scale per year from 2001 to 2019. This shows the contribution of the spatial random effects to the log of the dengue incidence rate using the drought severity - urban model.

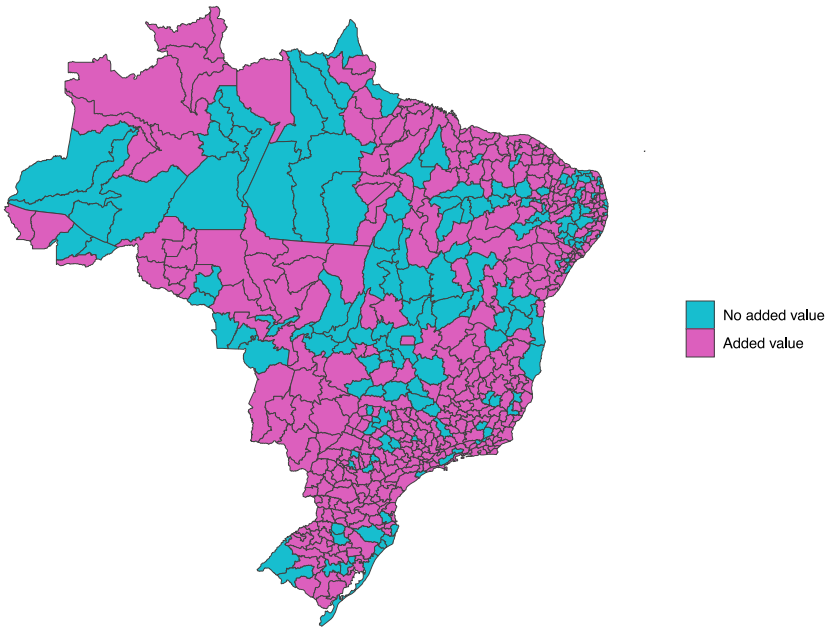

Figure A8: Added value of using drought severity - urban model compared to baseline model

Difference between mean absolute error (MAE) for the baseline model (state-specific monthly random effects and year-specific spatial random effects) and MAE for the drought severity - urban model (including a linear interaction between PDSI and urbanisation). Microregions with positive values (pink) suggest that capturing the nonlinear and delayed impacts of minimum temperature and drought severity index, interacted with level of urbanisation, improves the model in these areas. Microregions with negative values (blue) suggest that climate information did not improve the model fit and other unexplained factors may dominate space-time dynamics in these areas. The MAE of the drought severity - urban model (i.e., the model with the PDSI-urbanisation interaction) was smaller than the baseline model for 409 of the 558 (73%) microregions. When stratifying by geo-political region, the model performs best in the Southeast and South regions (Table A2)

Table A2. Added value from using the drought severity - urban model compared to the baseline model for each geo-political region

Difference between mean absolute error (MAE) for the baseline model (state-specific monthly random effects and year-specific spatial random effects) and MAE for the drought severity - urban model (including a linear interaction between the PDSI DLNM and urbanisation).

Region	Added value	Total	Proportion
North	37	64	58%
Northeast	130	188	69%
Southeast	135	160	84%
South	75	94	80%
Centre-West	32	52	62%
Brazil	409	558	73%

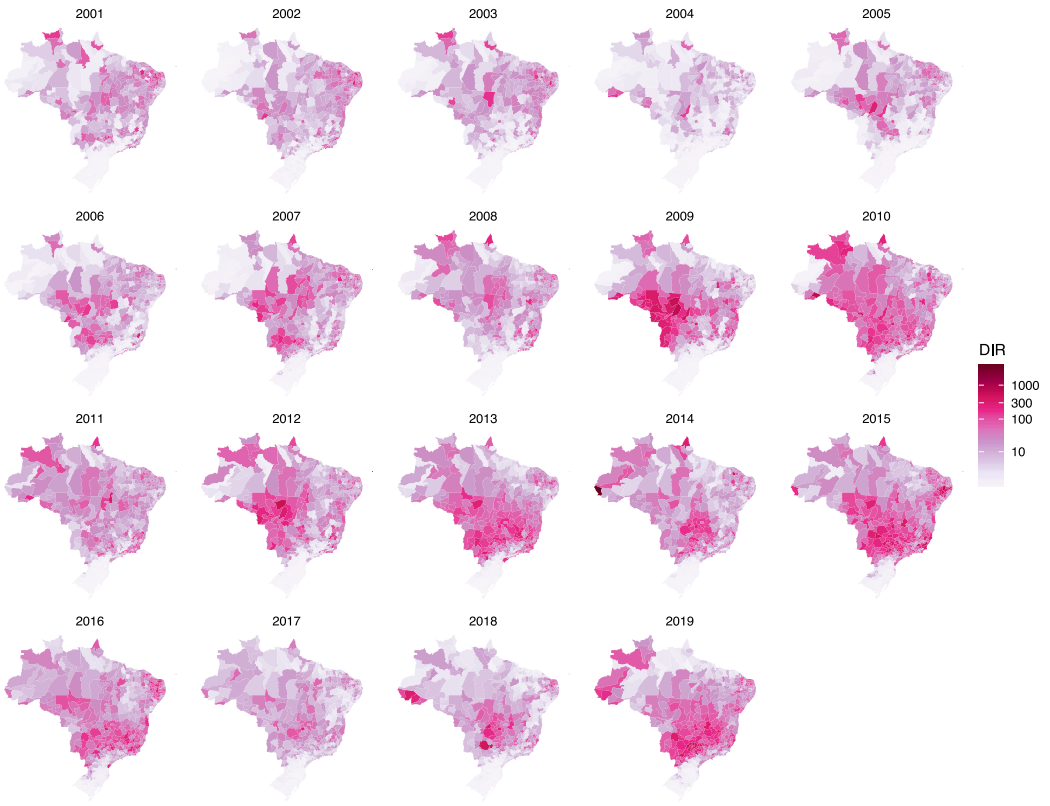

Figure A9: Posterior predictive mean dengue incidence rate 2001 – 2019

Posterior predictive mean dengue incidence rate (DIR) per 100 000 people per year from 2001 to 2019 for the 558 microregions in Brazil simulated from the drought severity - urban model (refitted 12 x 19 times, leaving out one month per year at a time).

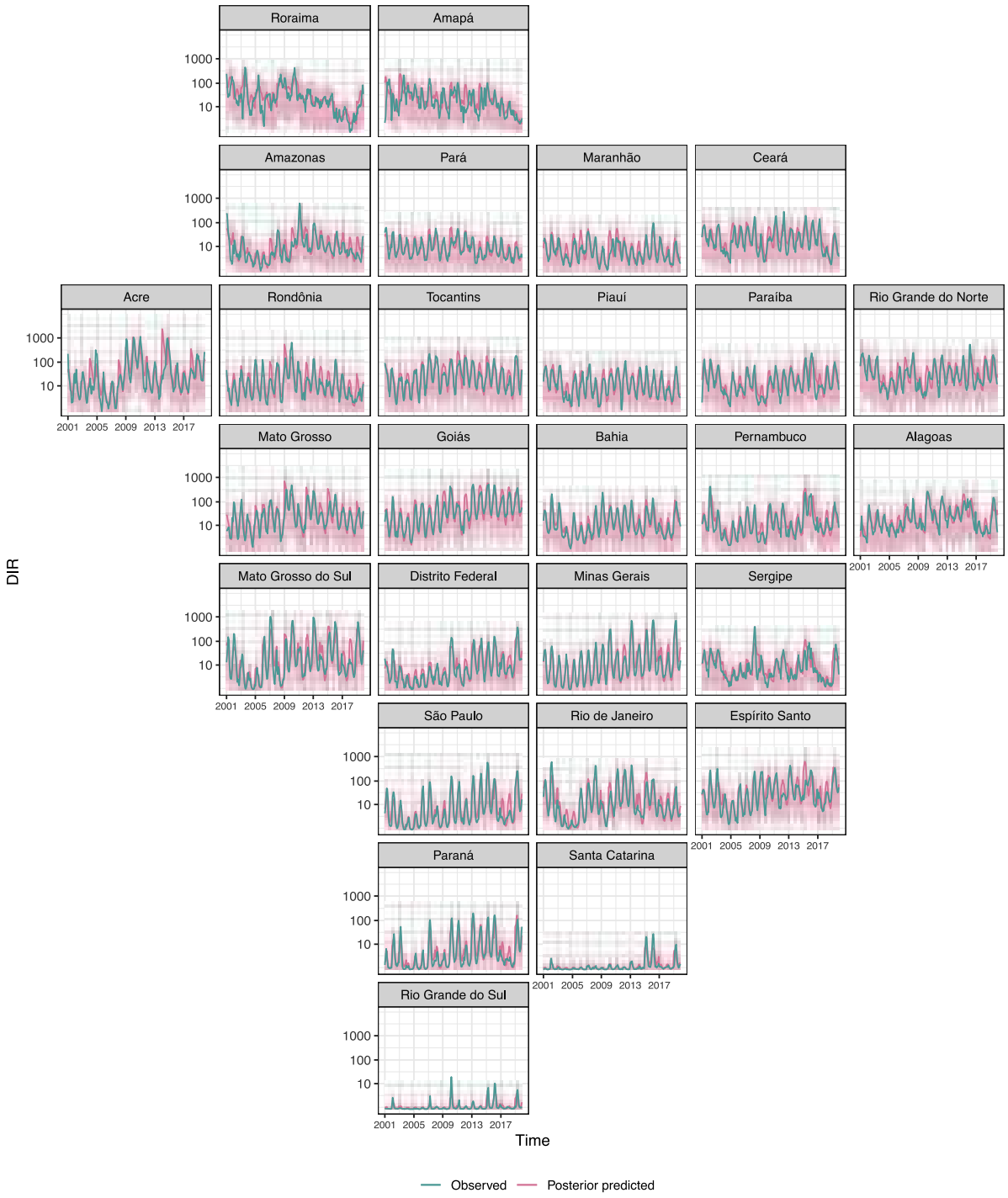

Figure A10: Observed versus posterior predictive dengue incidence rates per state

Mean observed dengue incidence rate (DIR) per 100 000 people (green curve) and corresponding posterior predictive mean (solid pink curve) and 95% prediction interval (shaded pink area) of DIR posterior predictive distributions from January 2001 to December 2019, simulated from the drought severity - urban model (refitted 12 x 19 times, leaving out one month per year at a time). for the 26 states and 1 federal district (Distrito Federal) in Brazil. States are ordered by their geographical location.

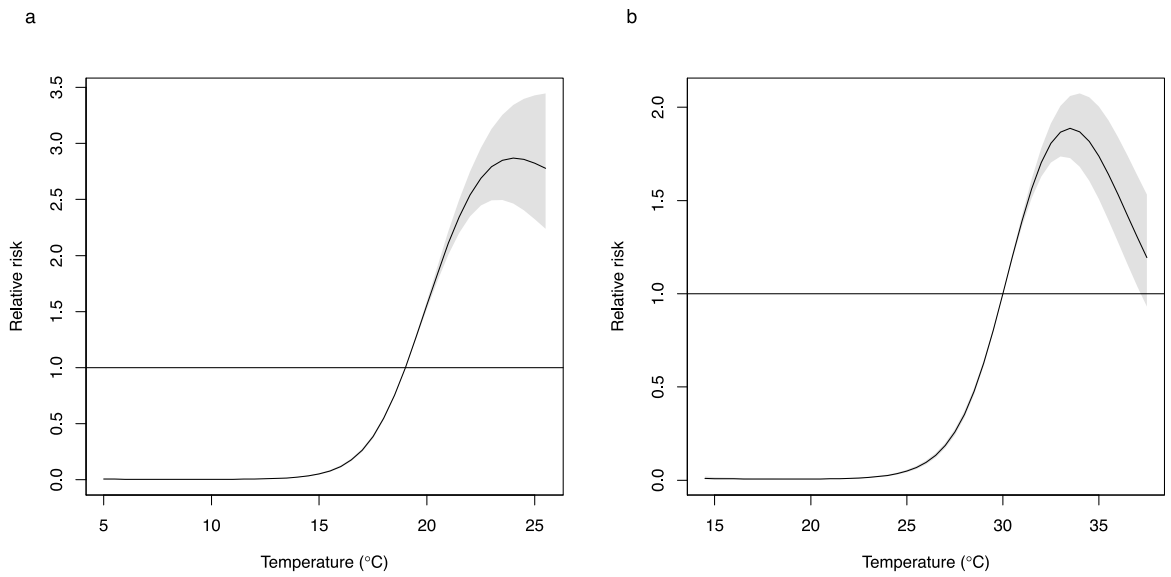

Fig A11. Cumulative exposure-response association for minimum and maximum temperature

Overall exposure–response association across all lags (zero to six months) between dengue relative risk and (a) minimum temperature relative to the overall mean minimum temperature of 19 °C and (b) maximum temperature relative to the overall mean maximum temperature of 29 °C. Results obtained from models including a DLNM for the Palmer drought severity index (with no interactions). The relative risk of dengue gradually increases with rising T_{min} above the mean and is greatest at the maximum T_{min} value of 25.5 °C. When replacing T_{min} with T_{max}, the relative risk increases with T_{max} until an optimum threshold of 34 °C, which is in line with optimum temperature thresholds reported in experimental studies.[21] The inclusion of minimum temperature resulted in improved model adequacy statistics compared to maximum temperature (see Table A1) and was used for further model exploration with drought severity and socio-economic interactions. Shaded areas represent 95% confidence intervals.

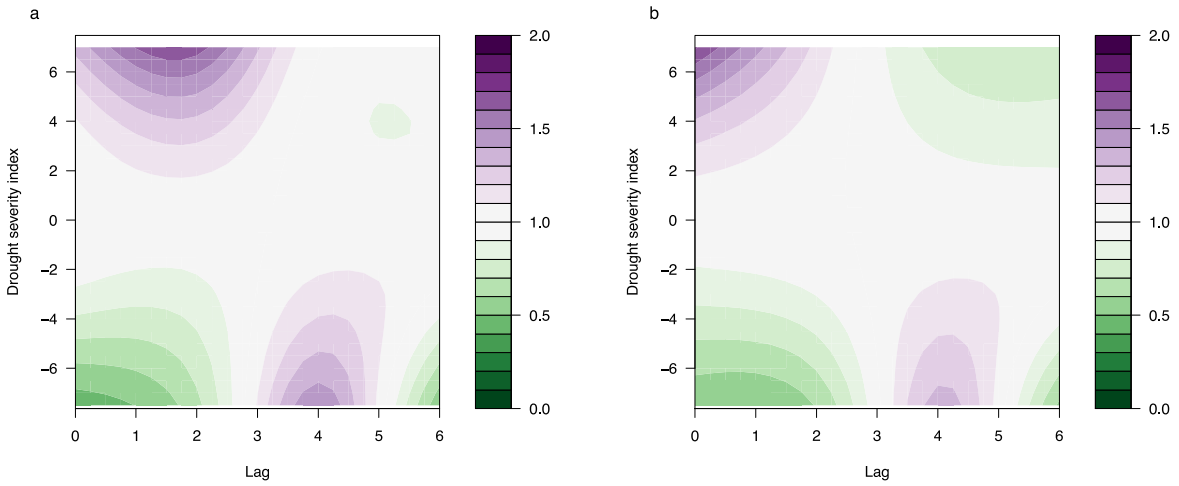

Fig A12. Association between risk of dengue and drought severity index at different time lags overall, and for high and low frequency of water supply shortages

Contour plots of the exposure–lag–response association between the Palmer drought severity index (PDSI) and dengue, relative to normal conditions (PDSI = 0) for microregions with (a) higher frequency of water supply shortages (upper quartile = 0.53) and (b) lower frequency of water supply shortages (lower quartile = 0.16) using the drought severity - water interaction model. The PDSI ranges from -10 (very dry) to + 10 (very wet), with values below -4 or above +4 considered ‘extreme’. The deeper the shade of purple the greater the increase in relative risk of dengue compared to normal conditions (PDSI = 0). The deeper the shade of green the greater the decrease in relative risk of dengue compared to normal conditions.

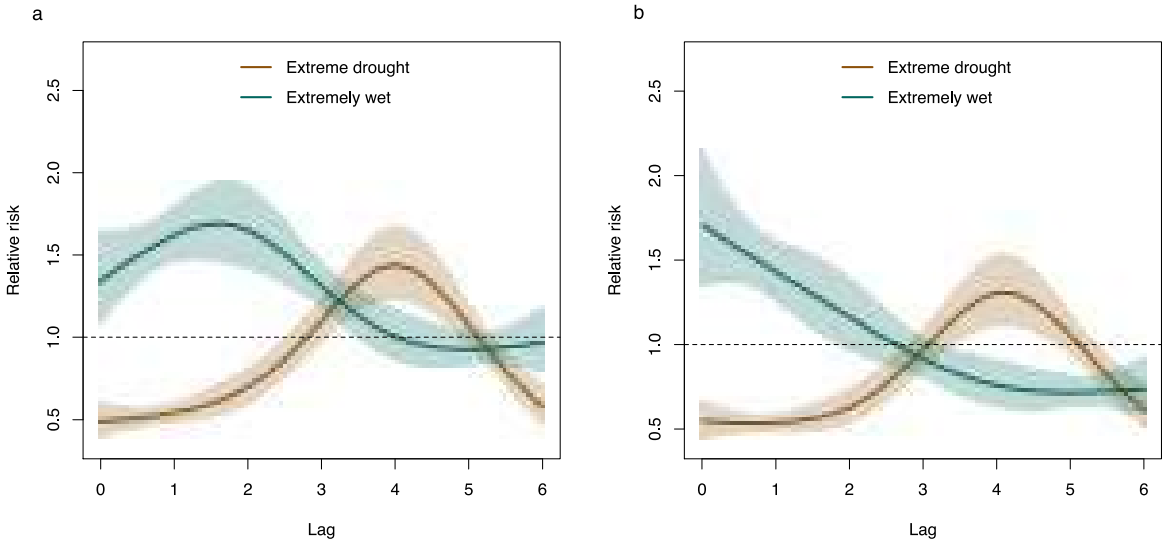

Fig A13. Dengue lag-response association for hydrometeorological hazard scenarios for high and low frequency water supply shortages

Lag–response association for extreme values of the Palmer drought severity index: exceptionally wet (PDSI = 7, green curve) and extreme drought (PDSI = -7, brown curve) conditions relative to normal conditions (PDSI = 0) at lags between zero and five months for areas with (a) high frequency of water supply shortages (upper quartile = 0.53) and (b) lower frequency of water supply shortages (lower quartile = 0.16) using the drought severity water interaction model. Shaded areas represent 95% confidence intervals.

Table A3. Risk of dengue for different hydrometeorological conditions by level of water shortage frequency

Relative risk (RR) of dengue compared to normal conditions (PDSI = 0) (i) overall (i.e., from the drought severity model without interactions), for (ii) high frequency water supply shortage (upper quartile = 0.53), (iii) intermediate frequency water supply shortage (median = 0.33) and (iv) low frequency water supply shortage (lower quartile = 0.16), from the drought severity – water shortage interaction model. The PDSI value at the maximum RR, the lag at the maximum (in months) and RR (and 95% confidence interval, CI) at the maximum are reported for both wet (PDSI > 0) and dry conditions (PDSI <= 0).

	Wet conditions			Dry conditions		
	PDSI at max	Lag at max (month)	RR (95% CI)	PDSI at max	Lag at max (month)	RR (95% CI)
i) Overall	7	1	1.56 (1.41, 1.73)	-7.5	4	1.43 (1.22, 1.67)
ii) High	7	2	1.68 (1.47, 1.92)	-7.5	4	1.48 (1.25, 1.75)
iii) Intermediate	7	0	1.54 (1.3, 1.84)	-7.5	4	1.4 2(1.21, 1.66)
iv) Low	7	0	1.71 (1.37, 2.15)	-7.5	4	1.34 (1.13, 1.6)

The PDSI index ranges from –10 (very dry) to 10 (very wet); values below –4 or above 4 are considered as extreme.

PDSI: Palmer Drought Severity Index; RR: relative risk; CI: confidence interval.

References

1 World Bank Group. World Bank indicators. 2019. https://data.worldbank.org/indicator/ (accessed June 7, 2020).

2 Ministério da Saúde. DATASUS - Departamento de Informática do SUS. Informações de Saúde (TABNET). http://www2.datasus.gov.br/DATASUS/index.php?area=02 (accessed June 7, 2020).

3 Ministério da Saúde. Secretaria de Vigilância em Saúde. Monitoramento dos casos de arboviroses urbanas transmitidas pelo Aedes Aegypti (dengue, chikungunya e zika), Semanas Epidemiológicas 1 a 20, 2020. Boletim Epidemiológico N° 21. Volume 51. 2020 https://antigo.saude.gov.br/images/pdf/2020/May/25/Boletim-epidemiologico-SVS-21.pdf.

4 Lowe R, Gasparrini A, Van Meerbeeck CJ, *et al.* Nonlinear and delayed impacts of climate on dengue risk in Barbados: A modelling study. *PLoS Med* 2018; **15**: 1–24.

5 Rue H, Martino S, Chopin N. Approximate Bayesian inference for latent Gaussian models by using integrated nested Laplace approximations. *J R Stat Soc Ser B Stat Methodol* 2009; **71**: 319–92.

6 Lindgren F, Rue H, others. Bayesian spatial modelling with R-INLA. *J Stat Softw* 2015; **63**: 1–25.

7 Schrödle B, Held L. A primer on disease mapping and ecological regression using INLA. *Comput Stat* 2011; **26**: 241–58.

8 Riebler A, Sørbye SH, Simpson D, H. Rue. An intuitive Bayesian spatial model for disease mapping that accounts for scaling. *Stat Methods Med Res* 2016; **25**: 1145–65.

9 Besag J, York J, Mollié A. Bayesian image restoration, with two applications in spatial statistics. *Ann Inst Stat Math* 1991; **43**: 1–20.

10 Simpson DP, Rue H, Riebler A, Martins TG, Sørbye SH. Penalising model component complexity: A principled, practical approach to constructing priors (with discussion). *Stat Sci* 2017; **32**: 1–28.

11 Gasparrini A. Modeling exposure–lag–response associations with distributed lag non-linear models. *Stat Med* 2014; **33**: 881–99.

12 Wells N, Goddard S, Hayes MJ. A Self-Calibrating Palmer Drought Severity Index. *J Clim* 2004; **17**: 2335–51.

13 Gasparrini A, Guo Y, Hashizume M, *et al.* Temporal variation in heat–mortality associations: a multicountry study. *Environ Health Perspect* 2015; **123**: 1200–7.

14 IBGE. Population Census 2010. 2020. https://www.ibge.gov.br/en/statistics/social/population/22836-2020-census-censo4.html?=&t=o-que-e (accessed May 24, 2020).

15 Spiegelhalter DJ, Best NG, Carlin BP, Van Der Linde A. Bayesian measures of model complexity and fit. *J R Stat Soc Ser B Stat Methodol* 2002; **64**: 583–639.

16 Held L, Schrödle B, Rue H avard. Posterior and cross-validatory predictive checks: a comparison of MCMC and INLA. In: Statistical modelling and regression structures. Springer, 2010: 91–110.

17 Gneiting T, Raftery AE. Strictly proper scoring rules, prediction, and estimation. *J Am Stat Assoc* 2007; **102**: 359–78.

18 Lowe R, Cazelles B, Paul R, Rodó X. Quantifying the added value of climate information in a spatio-temporal dengue model. *Stoch Environ Res Risk Assess* 2016; **30**: 2067–78.

19 Gelman A, Meng X-L, Stern H. Posterior predictive assessment of model fitness via realized discrepancies. *Stat Sin* 1996; **6**: 733–60.

20 Harris I, Osborn TJ, Jones P, Lister D. Version 4 of the CRU TS monthly high-resolution gridded multivariate climate dataset. *Sci Data* 2020; **7**: 1–18.

21 Mordecai EA, Caldwell JM, Grossman MK, *et al.* Thermal biology of mosquito-borne disease. *Ecol Lett* 2019.